JOURNAL OF AGRICULTURAL AND FOOD CHEMISTRY

Article

pubs.acs.org/JAFC

Probing the Binding of Insecticide Permethrin to Calf Thymus DNA by Spectroscopic Techniques Merging with Chemometrics Method

Yue Zhang, Guowen Zhang,* Yu Li, and Yuting Hu

State Key Laboratory of Food Science and Technology, Nanchang University, No. 235, Nanjing East Road, Nanchang 330047, Jiangxi, China

ABSTRACT: The binding of permethrin (PE) with calf thymus DNA (ctDNA) in physiological buffer (pH 7.4) was investigated by ultraviolet−visible (UV−vis) absorption, fluorescence, circular dichroism (CD), and Fourier transform infrared (FT−IR) spectroscopy merging with multivariate curve resolution−alternating least-squares (MCR−ALS) chemometrics approach. The MCR−ALS was applied to resolve the combined spectroscopic data matrix, which was obtained by UV−vis and fluorescence methods. The concentration profiles of PE, ctDNA, and PE−ctDNA complex and their pure spectra were then successfully obtained. The PE molecular was found to be able to intercalate into the base pairs of ctDNA as evidenced by decreases in resonance light-scattering signal and iodide-quenching effect and increase in ctDNA viscosity. The results of FT−IR spectra indicated that PE was prone to bind to G−C base pairs of ctDNA, and the molecular docking studies were used to validate and clarify the specific binding. The observed changes in CD signals revealed that the DNA turned into a more highly wound form of B-conformation. The calculated thermodynamic parameters, enthalpy change ($\Delta H°$) and entropy change ($\Delta S°$), suggested that hydrogen bonds and van der Waals forces played a predominant role in the binding of PE to ctDNA.

KEYWORDS: *permethrin, calf thymus DNA, multivariate curve resolution−alternating least-squares (MCR−ALS), binding mode, spectroscopy, molecular docking*

INTRODUCTION

DNA plays a major role in the life process because it carries heritage information and facilitates the biological synthesis of proteins and enzyme through replication and transcription of genetic information.[1] As DNA is quite often the main molecular target for studies with small molecules such as carcinogens, steroids, and several classes of drugs, the investigation of micromolecule−DNA interaction is of current interest and importance.[2,3] Generally, there are three modes for binding of small molecules with double-helix DNA in a noncovalent way: (i) electrostatic attractions with the anionic sugar phosphate backbone of DNA; (ii) interactions with the groove of DNA; and (iii) intercalation between the base pairs.[4] Among them, intercalative binding is considered as the most effective way to form DNA adduct, which might bring DNA damage. This is often the initiation phase of carcinogenicity when the damage gets away with the repair system.[5]

The use of pesticides in agriculture has brought huge economic benefit, but its negative effects also turn to be increasingly prominent, such as the pollution of food and environment. Pesticides can enter the human body through the food chain and the biological enrichment, which can cause accumulation of pesticide residue and trigger tissue lesions. Permethrin (PE) (Figure 1) is one of the pyrethroid insecticides and is widely used to prevent crop pests as well as hygiene and animal insect pests. However, Punareewattana et al. have demonstrated that topical exposure (the most relevant route of human exposure) of PE may be sufficient to alter function of the immune system.[6] Percutaneous absorption of varying levels of PE on mouse,[7] rhesus monkey,[8] rat, rabbit, dog, and human[9] has shown that exposure to PE by the dermal route can induce adverse immune effects in animals. Moreover,

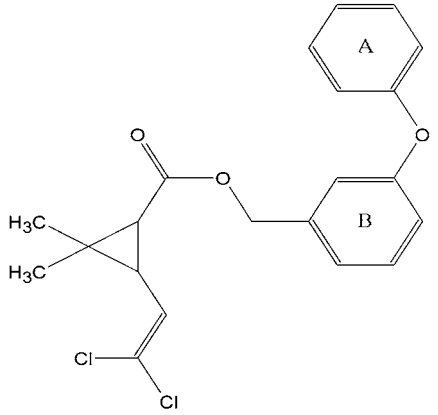

Figure 1. Structure of permethrin (PE).

the conclusions obtained through the genotoxicological experiment in rats indicated that subacute exposure of PE can increase the number of numberical chromosome aberrations.[10] Consequently, it is necessary to investigate the binding of PE with DNA to further understand the dangerous mechanism of PE in the body.

Spectroscopic methods including ultraviolet−visible (UV−vis) absorption, fluorescence, circular dichroism (CD), and Fourier transform infrared (FT−IR) spectroscopy are widely used to investigate the interaction of small molecules with DNA because of the advantages of sensitivity, reproducibility, and

Received: January 2, 2013
Revised: February 28, 2013
Accepted: February 28, 2013
Published: February 28, 2013

convenience.[11,12] However, for complex systems of more than two components, it is usually difficult to distinguish these existing species due to their response signals overlapping. In recent years, the application of chemometrics methods in the life sciences attracts much attention, because they can provide information well beyond that obtained by conventional methods. The multivariate curve resolution−alternating least-squares (MCR−ALS) method, which can overcome the limitation of response signals overlapping for each species in a complex system, has been used to analyze spectroscopic data from biomacromolecules' interactions with small molecules.[13] MCR−ALS is a soft-modeling method which is able to extract pure component spectra and the corresponding concentration profiles from spectroscopic data obtained from chemical reactions.[13] This method allows the analysis of more than one data matrix simultaneously, which reduces the number of possible solutions and inherent ambiguity in factor analysis. It is a good way to combine the spectroscopy method with trilinear chemometrics algorithms exploring the interaction of chemical substances with DNA even in the presence of interferents.[14]

In this work, the investigation of calf thymus DNA (ctDNA) interaction with PE was carried out in aqueous solution at physiological conditions using UV−vis absorption, fluorescence, CD, and FT−IR spectral approaches together with the MCR−ALS method. The binding mode and binding region of PE to ctDNA were estimated, and molecular docking was used to further validate the results. Furthermore, the MCR−ALS algorithm was employed to resolve the expanded spectroscopic data matrix which contained the UV−vis absorption and fluorescence spectral data collected from the PE−ctDNA mixtures. The concentration profiles of the three components (PE, ctDNA, and PE−ctDNA complex) in the reaction and the corresponding pure spectra were simultaneously extracted by MCR−ALS to explore the kinetic interaction process of PE with ctDNA.

MATERIALS AND METHODS

Materials. A stock solution (2.9×10^{-3} mol L^{-1}) of permethrin (Dr. Ehrenstorfer GmbH, Augsburg, Germany, purity ≥94.5%, nominal cis/trans 40:60) was prepared by dissolving its crystals in 95% (v/v) ethanol. Calf thymus DNA was purchased from Sigma-Aldrich Co., St. Louis, MO, and its stock solution was obtained by dissolving an appropriate amount of fibroid ctDNA in 0.1 mol L^{-1} NaCl solution and storing at 4 °C. The concentration of ctDNA in stock solution was 5.3×10^{-3} mol L^{-1} which was determined by UV absorption at 260 nm using a molar absorption coefficient ε_{260} = 6600 L $mol^{-1}cm^{-1}$.[15] The purity of ctDNA was checked by monitoring the ratio of the absorbance at 260 nm to that at 280 nm, and the solution gave a ratio of >1.8 at A_{260}/A_{280}, which indicated that ctDNA was sufficiently free from protein.[16] All solutions were adjusted with 0.05 mol L^{-1} Tris-HCl buffer of pH 7.4. All chemicals were of analytical reagent grade, and ultrapure water was used throughout the whole experiment.

Apparatus. The UV−vis absorption measurements were performed with a Shimadzu UV-2450 spectrophotometer (Shimadzu, Japan) using a 1.0 cm cell. The fluorescence and resonance light-scattering (RLS) spectra were measured on a Hitachi spectrofluorometer model F-7000 (Hitachi, Japan) equipped with a 150 W xenon lamp and a thermostat bath, using a 1.0 cm quartz cell. The CD spectra were recorded on a Bio-Logic MOS 450 CD spectrometer (Bio-Logic, France) using a 1.0 mm path length quartz cuvette. Infrared spectra were recorded with a FT−IR spectrometer (Thermo Nicolet-5700, U.S.) equipped with a germanium attenuated total reflection (ATR) accessory, a DTGS KBr detector, and a KBr beam splitter. The viscosity measurements were performed on a NDJ-79 viscosity meter (Yinhua Flowmeter Co., Ltd., Hangzhou, China). An electronic thermostat water bath (Shanghai Yuejin Medical Instrument Co., Shanghai, China) was used for controlling the temperature. A pHS-3C digital pH meter (Shanghai Exact Sciences Instrument Co., Ltd., Shanghai, China) was utilized to detect the pH values of the aqueous solutions. Millipore Simplicity water purification system (Millipore, Molsheim, France) was applied to produce freshly ultrapure water. All experiments, unless specified otherwise, were carried out at room temperature.

Fluorescence Spectra Measurements. PE (162 μL, 2.9×10^{-3} mol L^{-1}) was added to a 10 mL volumetric flask and diluted with pH 7.4 Tris-HCl buffer. An aliquot of this solution (3.0 mL) containing 4.7×10^{-5} mol L^{-1} PE was added to a 1.0 cm quartz cuvette, and then ctDNA was added to this solution at different concentrations in the range of 0−8.80×10^{-5} mol L^{-1}. These well-mixed solutions were allowed to stand for 4 min to equilibrate, and the fluorescence emission spectra were then measured at different temperatures (292, 298, 304, and 310 K) in the wavelength range of 290−500 nm with exciting wavelength at 274 nm. The widths of both the excitation and emission slits were set at 2.5 nm.

Experiments To Get the Expanding Data Matrix for MCR−ALS. UV−vis absorption and fluorescence spectroscopy were applied to monitoring the interaction process of PE with ctDNA. Two different experiments to get the expanding data matrix for MCR−ALS were carried out in pH 7.4 Tris-HCl buffer at room temperature. Experiment 1: the concentration of PE was fixed at 5.9×10^{-5} mol L^{-1}, and different amounts of ctDNA (0−1.4×10^{-4} mol L^{-1} at an interval of 5.4×10^{-6} mol L^{-1}, total 27 solutions) were added to the solution. Experiment 2: the concentration of ctDNA was kept at 5.0×10^{-5} mol L^{-1}, and various amounts of PE (0−3.38×10^{-5} mol L^{-1} at an interval of 1.3×10^{-6} mol L^{-1}, total 27 solutions) were added. After each addition the solutions were allowed to stand for 4 min, and then the UV−vis absorption spectra (200−350 nm; scanned every 1 nm) and fluorescence (284−400 nm; excitation wavelength at 274 nm; scanned every 1 nm) spectra were collected respectively. Therefore, four data matrices $\mathbf{D}_{UV}^{PE}$ (27 × 151), $\mathbf{D}_{F}^{PE}$ (27 × 117), $\mathbf{D}_{UV}^{ctDNA}$ (27 × 151), and $\mathbf{D}_{F}^{ctDNA}$ (27 × 117) were obtained from these measurements, and a column- and row-wise expanded data matrix was constructed.

Resonance Light-Scattering (RLS) Spectra. A 3.0 mL solution containing 6.2×10^{-7} mol L^{-1} PE was added to the quartz cuvette and then titrated by successive additions of ctDNA (to give a concentration range from 0 to 2.65×10^{-5} mol L^{-1}). The solution was mixed sufficiently and stood for 4 min before measurements. The RLS spectra were obtained by synchronous scanning on the spectrofluorometer ($\Delta\lambda$ = 0 nm) with the wavelength range of 200−700 nm at room temperature. Both the slit widths of excitation and emission were set at 10 nm.

Viscosity Measurements. Viscometric titrations were performed in a viscometer, which was kept in a constant temperature bath at 25 ± 0.1 °C. An appropriate amount of PE was added into the viscometer to give a certain r (r = [PE]/[ctDNA]) value while keeping the concentration of ctDNA constant. After a thermal equilibrium was achieved (20 min), the flow times of the solutions through the capillary were

repeatedly measured at least three times with an accuracy of ±0.2 s using a digital stopwatch. The mean values of the replicated measurements were used to evaluate the average relative viscosity of the solutions. The data were presented as $(\eta/\eta_0)^{1/3}$ versus r,[17] while η_0 and η represent the viscosity of ctDNA in the absence and presence of PE, respectively. Viscosity values were calculated from the observed flow time of ctDNA containing solutions (t) and corrected for buffer solution (t_0), $\eta = (t - t_0)/t_0$.

CD Studies. The CD spectra of ctDNA incubated with PE at molar ratios ([PE]/[ctDNA]) of 0, 1, and 2 were measured at wavelengths between 220 and 320 nm with 0.1 nm step resolution and averaged over three scans recorded at a speed of 120 nm min^{-1}. The optical chamber of the CD spectrometer was deoxygenated with dry nitrogen before use and kept in a nitrogen atmosphere during experiments. Scans were accumulated and automatically averaged. The CD measurements were performed in pH 7.4 Tris-HCl buffer at room temperature, all observed CD spectra were corrected for the buffer signal, and results were expressed as circular dichroism in millidegree.

FT−IR Spectra Measurements. FT−IR spectra were recorded after 2 h incubation of PE with ctDNA at molar ratios of PE to ctDNA of 1:200, 1:100, 1:50, and 1:25 in pH 7.4 Tris-HCl buffer. All spectra were measured over the spectral range 1800−800 cm^{-1} with a resolution of 4 cm^{-1} and 64 scans. The water subtraction was carried out using H_2O solution at pH 7.4 as a reference. A good water subtraction was considered to be achieved if there was a flat baseline around 2200 cm^{-1}, where the water combination mode was located. This method yields a rough estimate of the subtraction scaling factor, but it removes the spectral features of water in a satisfactory way.[18]

The difference spectra [(ctDNA + PE) − PE solution] were obtained using a sharp ctDNA band at 968 cm^{-1} as an internal reference. The plots of the relative intensity (R) of several peaks of ctDNA in-plane vibrations related to base pairs and phosphate stretching vibrations versus the molar ratios of PE to ctDNA were obtained after peak normalization using

$$R_i = \frac{I_i}{I_{968}} \tag{1}$$

where I_i is the intensity of absorption peak at i cm^{-1} for free ctDNA and its complex at different concentration of PE, and I_{968} is the intensity of the 968 cm^{-1} peak (internal reference).

Molecular Modeling Studies. The 3D structure of PE was generated in Sybyl ×1.1 (Tripos Inc., St. Louis, U.S.), and its energy-minimized conformation was obtained with the help of the MMFF94 force field using MMFF94 charges. The rotatable bonds in the ligand were assigned with AutoDock Tools, and the ligand docking was performed with the AutoDock 4.2 Lamarckian Genetic Algorithm (LGA). The B-DNA crystal structure used for the docking studies was obtained from the Protein Data Bank with identifier 453D.[19] The DNA file prepared for docking removed water; meanwhile, essential hydrogen atoms along with Gasteiger charges were added with the aid of AutoDock Tools.[20,21] After ctDNA was enclosed in the grid defined with 0.375 Å spacing, other miscellaneous parameters were assigned the default values given by AutoDock. The output from AutoDock was rendered with PyMol.

Chemometrics Method: Multivariate Curve Resolution−Alternating Least-Squares (MCR−ALS). Multivariate curve resolution−alternating least-squares (MCR−ALS) has been applied to resolve multiple component responses in unknown mixtures. The goal of this self-modeling method is to decompose composite-measured profiles such as spectra into the different pure profiles for each species in a mixture and investigate the molecular complex formation processes.[22,23] A short description of the MCR−ALS is given here.

The MCR method facilitates a bilinear decomposition of the experimental data matrix with the use of the following model

$$\mathbf{D} = \mathbf{C}\mathbf{S}^{\mathrm{T}} + \mathbf{E} \tag{2}$$

where $\mathbf{C}$ is the matrix that describes the changes in concentration of the existing species, $\mathbf{S}^{\mathrm{T}}$ is the matrix that contains the pure spectra profiles of the species, and $\mathbf{E}$ is the residual matrix.

The MCR procedure consists of the following steps: (i) Data arrangement: the data from each experiment are collected in matrix $\mathbf{D}$ ($r \times c$)—the r rows contain the recorded spectra, and the c columns are the wavelengths. $\mathbf{C}$ ($r \times n$) is the matrix which contains the contribution of the n spectroscopically active species and changes in the different r rows (concentration profiles). $\mathbf{S}^{\mathrm{T}}$ ($n \times c$) is the matrix which describes how the instrumental response of these n species changes in the c columns of the data matrix (pure spectral profiles). $\mathbf{E}$ ($r \times c$) is the residual matrix with the data variance unexplained by the product $\mathbf{C} \times \mathbf{S}^{\mathrm{T}}$. (ii) Determination of the number of components: The number N is estimated by rank analysis with the use of singular value decomposition (SVD),[24] which is a related technique based on factor analysis—evolving factor analysis (EFA).[25] The rank of the matrix calculated by the method is assumed to be the number of chemical species in the system. (iii) Initial estimates of the concentration profiles and spectra are generally obtained from EFA plots[25,26] or the SIMPLISMA approach,[27] respectively. MCR−ALS is applied to matrix $\mathbf{D}$ using either the generated initial estimated concentration profiles or spectra. (iv) ALS optimization: The ALS optimization procedure is an iterative method, which starts with an initial estimation of the $\mathbf{C}$ data matrix obtained from EFA for the considered N species. It is used to obtain the matrix of the pure spectra $\mathbf{S}^{\mathrm{T}}$ and the matrix of species distribution $\mathbf{C}$, which best fit the experimental data matrix, $\mathbf{D}$.

The powerful extension of MCR−ALS was developed to deal with multiple data matrices simultaneously, and it is possible to resolve several measurement techniques by augmenting the input matrix appropriately.[28] There were two types of experiments and two types of spectroscopic methods in this paper; thus, a total of four data matrices were obtained. The final model used for the extended MCR−ALS analysis is

$$\begin{bmatrix} \mathbf{D}_{\mathrm{UV}}^{\mathrm{PE}} & \mathbf{D}_{\mathrm{F}}^{\mathrm{PE}} \\ \mathbf{D}_{\mathrm{UV}}^{\mathrm{ctDNA}} & \mathbf{D}_{\mathrm{F}}^{\mathrm{ctDNA}} \end{bmatrix} = \begin{bmatrix} \mathbf{C}^{\mathrm{PE}} \\ \mathbf{C}^{\mathrm{ctDNA}} \end{bmatrix} \times \begin{bmatrix} \mathbf{S}_{\mathrm{UV}}^{\mathrm{T}} & \mathbf{S}_{\mathrm{F}}^{\mathrm{T}} \end{bmatrix} + \begin{bmatrix} \mathbf{E}_{\mathrm{UV}}^{\mathrm{PE}} & \mathbf{E}_{\mathrm{F}}^{\mathrm{PE}} \\ \mathbf{E}_{\mathrm{UV}}^{\mathrm{ctDNA}} & \mathbf{E}_{\mathrm{F}}^{\mathrm{ctDNA}} \end{bmatrix} \tag{3}$$

where the matrix with superscript PE refers to the experiment with the concentration of PE constant and the matrix with superscript ctDNA refers to the experiment with the concentration of ctDNA constant. All of four individual data matrices are simultaneously analyzed using eq 3. In the equation, $[[\mathbf{D}_{\mathrm{UV}}, \mathbf{D}_{\mathrm{F}}]^{\mathrm{PE}}; [\mathbf{D}_{\mathrm{UV}}, \mathbf{D}_{\mathrm{F}}]^{\mathrm{ctDNA}}]$ is the row- and columnwise augmented experimental data matrix that contains all the data obtained from the two different spectroscopic

experiments, $[\mathbf{C}^{PE}; \mathbf{C}^{ctDNA}]$ represents the columnwise augmented concentration matrix while $[\mathbf{S}_{UV}, \mathbf{S}_F]^T$ represents the row-wise augmented spectral matrix, and $[[\mathbf{E}_{UV}, \mathbf{E}_F]^{PE}; [\mathbf{E}_{UV}, \mathbf{E}_F]^{ctDNA}]$ is the row- and columnwise augmented error matrix corresponding to the two different spectroscopic experiments with dimensions $(\mathbf{N}^{PE} + \mathbf{N}^{ctDNA}) \times (\mathbf{N}_{UV} + \mathbf{N}_F)$.

RESULTS AND DISCUSSION

Absorption Spectra and Fluorescence Spectra of Interaction between PE and ctDNA. Figure 2A displays

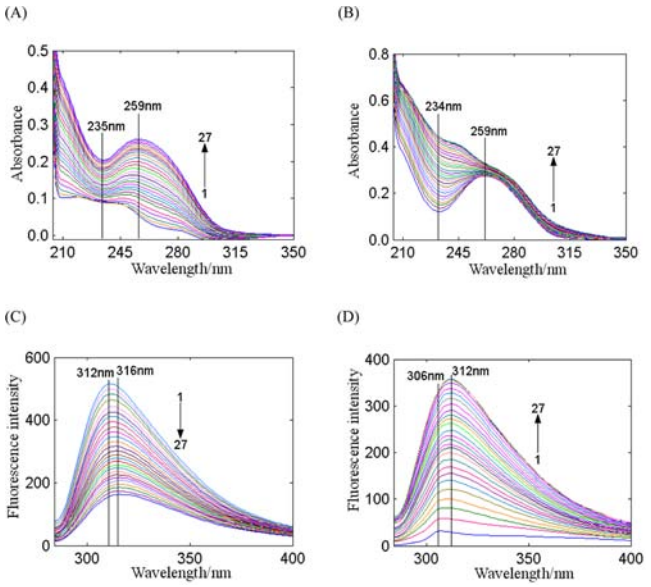

Figure 2. Spectra obtained from different experiments. Experiment 1: (A) UV−vis ($\mathbf{D}_{UV}^{PE}$) and (C) fluorescence ($\mathbf{D}_F^{PE}$), c(PE) = 5.9 × 10^{-5} mol L^{-1}, and c(ctDNA) = 0, 0.54, 1.08, ..., 14.04 × 10^{-5} mol L^{-1} for curves 1−27, respectively. Experiment 2: (B) UV−vis ($\mathbf{D}_{UV}^{ctDNA}$) and (D) fluorescence ($\mathbf{D}_F^{ctDNA}$), c(ctDNA) = 5.0 × 10^{-5} mol L^{-1}, and c(PE) = 0, 0.13, 0.26, ..., 3.38 × 10^{-5} mol L^{-1} for curves 1−27, respectively.

the UV−vis absorption spectra of PE in the presence of different concentrations of ctDNA. PE exhibited three absorption bands at around 215, 245, and 283 nm, respectively. With increasing amounts of ctDNA, the absorption intensity of PE at 245 increased gradually with a significant red shift (from 245 to 259 nm, corresponding to curves from 1 to 27). On the other hand, the absorption peak of ctDNA at 259 nm which resulted from the strong absorption of purine and pyrimidine bases in DNA[29] showed slight increase in intensity together with a valley at around 234 nm enhanced greatly with increasing amounts of PE (Figure 2B). Moreover, the fluorescence band of PE at 312 nm was quenched by increasing concentrations of ctDNA (Figure 2C), and a red-shift from 312 to 316 nm was observed clearly. Whereas only a weak fluorescence spectrum of ctDNA with a slight band at 306 nm could be found, the augment of PE enhanced its intensity and shifted it to 312 nm (Figure 2D).

The obtained UV and fluorescence spectral profiles were intricate and high spectral overlap existed for each species. It is difficult to recognize the spectrum of the PE−ctDNA complex and estimate the concentration changes of reaction components during the titration process by conventional methods. Therefore, the four spectral data matrices were combined and submitted to MCR−ALS analysis in an attempt to extract the pure spectrum of each reaction component and the associated concentration profiles.

Decomposition of the Expanded UV and Fluorescence Data Matrix by MCR−ALS. The expanded data matrix was processed by the MCR−ALS approach as described above. The number of significant factors, related to the chemical species, was evaluated with the application of the SVD method to the augmented data matrix.[23] The extracted first four eigenvalues turned out to be 102.32, 31.62, 10.23, and 1.99, indicating that there were essentially three significant factors for the prediction of three separate chemical components in the system, i.e., PE, ctDNA, and PE−ctDNA complex. In general, the MCR−ALS analysis has to be initialized with estimates of the pure spectra or concentrations for the three postulated species from the seriously overlapped spectra. Figure 3A−B

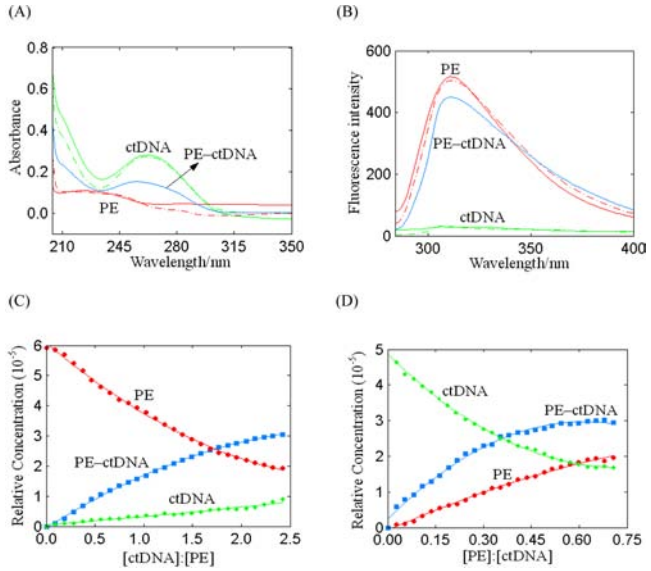

Figure 3. Results obtained from the simultaneous analysis of the UV−vis and fluorescence data of the two experiments by MCR−ALS. (A) Recovered UV−vis spectra and (B) recovered fluorescence spectra (solid line, recovered spectra; dashed line, measured spectra). Recovered concentration profiles for experiment 1 (C) and experiment 2 (D).

displays the pure UV−vis and fluorescence spectra recovered for different species, which correspond to $\mathbf{S}_{UV}^T$ and $\mathbf{S}_F^T$, respectively. The resolved spectra (solid line) of the free PE and ctDNA agreed well with the measured counterparts (dashed line). It should be noted that the UV−vis and fluorescence spectra for the PE−ctDNA complex (solid line of PE−ctDNA in Figure 3A−B), which were difficult to observe by conventional methods, were obtained with the use of MCR−ALS. The good agreement between the predicted and the measured spectral profiles suggested that the concentration profiles were correctly resolved.[13] The concentration profiles of PE, ctDNA, and PE−ctDNA complex were obtained by analyzing the expanded UV and fluorescence data matrix using the MCR−ALS model. It can be seen from Figure 3C that with the addition of ctDNA, the concentration of PE−ctDNA complex increased gradually accompanied by the decrease of the concentration of PE, and some free ctDNA was still present in the reaction system. In contrast, an increasing tendency of the concentration of PE−ctDNA complex and a decreasing tendency of the concentration of

dx.doi.org/10.1021/jf400017f | J. Agric. Food Chem. 2013, 61, 2638−2647

ctDNA were observed with increasing concentration of PE (Figure 3D). Summing up the results obtained above, it was concluded that PE bound to ctDNA and formed the PE−ctDNA complex.

RLS Spectra. The RLS spectra of PE and PE−ctDNA system in pH 7.4 Tris-HCl buffer are shown in Figure 4. It can

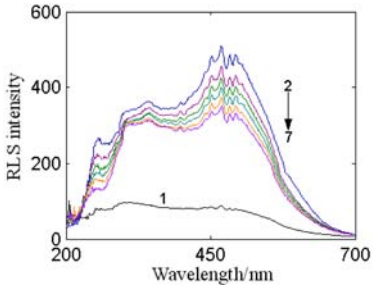

Figure 4. RLS spectra of the PE−ctDNA system at pH 7.4 and room temperature. c(PE) = 6.2 × 10^{-7} mol L^{-1}, and c(ctDNA) = 0, 0.53, 1.06, 1.59, 1.20, and 2.65 × 10^{-5} mol L^{-1} for curves 2−7, respectively. Curve 1 shows the RLS spectrum of ctDNA only, c(ctDNA) = 5.3 × 10^{-6} mol L^{-1}.

be seen that RLS intensity of PE was strong in the absence of ctDNA, and a significant reduction in the RLS intensity came into being as a result of increasing concentration of ctDNA. Previous studies have shown that fuchsin basic (FB) can interact with ctDNA via two different ways: long-range assembly or intercalation. When long-range assembly of FB on the molecular surface of ctDNA occurs, the RLS intensity of FB can be greatly enhanced upon the addition of ctDNA, and if FB interacts with ctDNA in an intercalative mode, the RLS signal of FB should be decrease with the addition of ctDNA.[30] Therefore, it was reasonable to assume the decrease of the RLS signal of PE might be due to the intercalation into ctDNA, and the diameter of the complex substantially exceeded the appropriate range in RLS theory, which induced light emission change from light scattering to light reflection, and thus the RLS intensity of the analytical system decreased noticeably.[31]

Fluorescence Spectroscopic Studies. Fluorescence spectroscopy was usually used to characterize the binding characteristics of the chromophore with other molecules. Figure 5A shows the fluorescence emission spectra of PE in the absence and presence of ctDNA. It can be observed that PE presented a strong fluorescence emission peak between 290 and 500 nm with an excitation wavelength at 274 nm. Upon the addition of ctDNA, the fluorescence peak of PE showed significant decrease with a slight red-shift, suggesting that the PE moleculars entered the DNA-stacking region with a lower polarity.[32]

It is well-known that there mainly exist two kinds of quenching processes, dynamic and static quenching. Dynamic quenching refers to a process that the fluorophore and the quencher come into contact during the transient existence of the excited state whereas the static quenching refers to fluorophore−quencher complex formation. Dynamic and static quenching can be distinguished by their different dependence on temperature.[33] Dynamic quenching depends upon diffusion. Since higher temperatures result in larger diffusion coefficients, the bimolecular quenching constants are expected to increase with increasing temperature. In contrast, increased temperature is likely to result in decreased stability of complex and thus lower the values of static quenching constants.[34] To clarify

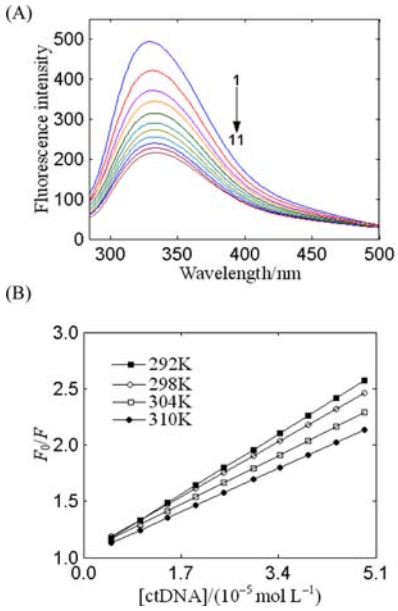

Figure 5. (A) Fluorescence spectra of PE in the presence of ctDNA at different concentrations (pH 7.4, T = 298 K; λ_{ex} = 274 nm). c(PE) = 4.7 × 10^{-5} mol L^{-1}; c(ctDNA) = 0, 0.88, 1.75, 2.64, 3.52, 4.40, 5.28, 6.16, 7.04, 7.92, and 8.80 × 10^{-5} mol L^{-1} for curves 1−11, respectively. (B) The Stern−Volmer plots for the fluorescence quenching of PE by ctDNA at different temperatures.

quenching mechanism, fluorescence quenching spectra were measured at different temperatures.

For the dynamic quenching, the mechanism can be described by the Stern−Volmer equation

$$\frac{F_0}{F} = 1 + K_{SV}[Q] = 1 + K_q\tau_0[Q] \quad (4)$$

where F_0 and F are the fluorescence intensities in the absence and presence of ctDNA, respectively. K_{SV} is the Stern−Volmer quenching constant, which was determined by linear regression of a plot of F_0/F against [Q]. K_q is the quenching rate constant of biomolecule, τ_0 is the average lifetime of the fluorophore without quencher, the value of τ_0 of the biopolymer is 10^{-8} s, and [Q] is the concentration of DNA.

Plots of F_0/F versus [ctDNA] at different temperatures (292, 298, 304, and 310 K) are shown in Figure 5B by using eq 4; the corresponding *K*sv values for the binding of PE with ctDNA were obtained, and the results are listed in Table 1. The values of K_{SV} showed a decrease with increasing temperature, indicating that the probable quenching mechanism of PE−ctDNA interaction was a static quenching procedure.

According to the modified Stern−Volmer equation,[35] the association constant of PE−ctDNA interaction can be estimated

$$\frac{F_0}{F_0 - F} = \frac{1}{f_a K_a}\frac{1}{[Q]} + \frac{1}{f_a} \quad (5)$$

where K_a is the modified Stern−Volmer association constant for the accessible fluorophores and f_a is the fraction of accessible fluorescence. The dependence of $F_0/(F_0 - F)$ on the reciprocal value of the quencher concentration $1/[Q]$ is linear. The constant K_a is the quotient of an ordinate $1/f_a$ and slope $1/f_aK_a$. The calculated K_a values at four different temperatures are presented in Table 1, and it can be seen that the decreasing

Table 1. Quenching Constants (K_{SV}), Binding Constants (K_a), and Relative Thermodynamic Parameters of the PE−ctDNA System at Different Temperatures

T (K)	K_{SV} ($\times 10^4$ L mol^{-1})	R^a	K_a ($\times 10^4$ L mol^{-1})	R^b	$\Delta H°$ (kJ mol^{-1})	$\Delta S°$ (J K^{-1} mol^{-1})	$\Delta G°$ (kJ mol^{-1})
292	3.12 ± 0.01	0.9991	4.16 ± 0.05	0.9987	−35.51 ± 0.15	−32.34 ± 0.57	−26.07 ± 0.04
298	2.89 ± 0.01	0.9989	3.70 ± 0.02	0.9998			−25.87 ± 0.04
304	2.54 ± 0.01	0.9975	3.03 ± 0.07	0.9983			−25.68 ± 0.05
310	2.29 ± 0.01	0.9989	1.72 ± 0.14	0.9962			−25.48 ± 0.05

$^a R$ is the correlation coefficient for the K_{SV} values. $^b R$ is the correlation coefficient for the K_a values.

trend of K_a with increasing temperature was in accordance with K_{SV}'s dependence on temperature as discussed above, which further confirmed that the fluorescence quenching of PE was static quenching.

Determination of Thermodynamic Parameters and the Nature of Binding Forces. The thermodynamic parameters dependent on temperatures were analyzed in order to further characterize the interaction forces between PE and ctDNA. The interaction forces between small molecules and biomolecules mainly include hydrogen bonds, van der Waals force, hydrophobic force, and electrostatic interactions. The thermodynamic parameters of binding reaction are the main evidence for confirming the binding force. Enthalpy change ($\Delta H°$) and entropy change ($\Delta S°$) of the binding reaction were used to determine the binding force which plays a main role during the interaction process.

If $\Delta H°$ does not vary significantly over the temperature range studied, then its value and that of $\Delta S°$ can be determined from the van't Hoff equation

$$\log K_a = -\frac{\Delta H°}{2.303RT} + \frac{\Delta S°}{2.303R} \quad (6)$$

$$\Delta G° = \Delta H° - T\Delta S° \quad (7)$$

where K_a is the association constant at the four temperatures (292, 298, 304, and 310 K) and R is the gas constant. The values of $\Delta H°$ and $\Delta S°$ were obtained from the slope and intercept of the linear van't Hoff plot based on log K_a versus $1/T$. The free energy change ($\Delta G°$) was then evaluated from eq 7. Table 1 lists the thermodynamic parameters for the interaction of PE with ctDNA. The negative signal for $\Delta G°$ indicated that the PE−ctDNA interaction was spontaneous. The negative values of $\Delta H°$ and $\Delta S°$ revealed that the reaction was exothermic and enthalpy favored, which suggested the binding was driven mainly by hydrogen bond and van der Waals forces and considered evidence for intercalative binding.[36,37]

Iodide-Quenching Studies. Iodide-quenching experiments can provide further support for the intercalative binding of PE to ctDNA. A highly negatively charged quencher is expected to be repelled by the negatively charged phosphate backbone of ctDNA. When a small molecule interacts with DNA via intercalative mode, the molecule should be protected from being quenched by anionic quencher; however, different from intercalation, groove binding provides much less protection for the bound molecule.[38] The plots of F_0/F versus [KI] in the absence and presence of ctDNA are shown in Figure 6 based on the Stern−Volmer equation. As shown in Figure 6, in the absence of ctDNA, the fluorescence of PE was efficiently quenched by I^- ion, resulting in a linear Stern−Volmer plot of larger slope (K_{SV} = 108.25 L mol^{-1}). However, in the presence of ctDNA, the slope of the plot (K_{SV} = 31.79 L mol^{-1}) was remarkably decreased. The results implied that the

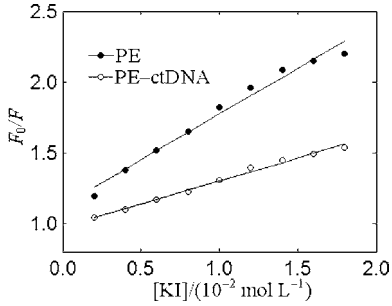

Figure 6. Fluorescence-quenching plots of PE by KI in the absence and presence of ctDNA at pH 7.4 and room temperature. c(PE) = 4.7 × 10^{-5} mol L^{-1} and c(ctDNA) = 4.4 × 10^{-5} mol L^{-1}.

bound PE molecules intercalated into the base pairs of ctDNA which induced a decrease in the iodide-quenching effect.

Viscosity Measurements. Viscosity experiments are an effective tool to decide the binding mode of small molecules and DNA. Thus, to further clarify the interaction of PE with ctDNA, viscosity measurements were performed. A classical intercalation binding demands the space of adjacent base pairs to be large enough to accommodate the bound ligand and to elongate the double helix, which results in an increase of DNA viscosity.[39] In contrast, a partial nonclassical intercalation of the ligand would decrease the DNA viscosity. There is little effect on the viscosity of DNA if nonintercalation binding occurs in the binding process.[40,41] Figure 7 shows that the relative

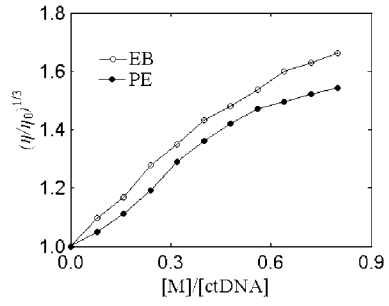

Figure 7. Effects of increasing amounts of PE and ethidium bromide (EB) on the relative viscosity of ctDNA at pH 7.4 and 298 K. c(ctDNA) = 5.0 × 10^{-5} mol L^{-1}.

viscosity of ctDNA increased significantly with increasing concentrations of PE, which was similar to the increasing trend of ctDNA viscosity upon the addition of ethidium bromide (EB), a typical DNA intercalator. Combined with above conclusions, such behavior further indicated that the binding mode of PE to ctDNA should be intercalation.

CD Studies. The changes in CD signals of DNA observed on interaction with small molecules may be assigned to the corresponding changes in DNA conformation. Figure 8 displays the CD spectra of different molar ratios of PE to ctDNA

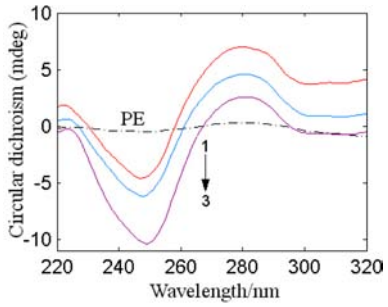

Figure 8. Circular dichroism spectra of ctDNA in the presence of increasing amounts of PE at pH 7.4 and room temperature. c(PE) = 5.0×10^{-4} mol L^{-1} (dashed line); c(ctDNA) = 5.0×10^{-4}. The molar ratios of PE to ctDNA were 0:1, 1:1, and 2:1 for curves 1−3, respectively.

([PE]/[ctDNA]). Two major peaks between 220 and 320 nm, 245 nm (negative) and 275 nm (positive), are characteristic peaks for B-conformation of DNA. The negative peak at 245 nm and positive peak at 275 nm are attributed to right-handed helicity and stacking of the bases of B-DNA, respectively.[42] It was observed that the intensity of negative peak increased and positive peak decreased without any significant shift in the peaks position after binding with PE, suggesting that ctDNA became a more highly wound form of B-DNA in the presence of PE.[43] This variant of B-DNA structures differs from normal in the number of base pairs per helix turn.[44]

FT−IR Studies. The infrared spectral features of double helical structure of ctDNA associated with the binding of PE can provide useful information on the specific binding region of PE binding to ctDNA and clarify the influence of PE on ctDNA phosphate skeleton and base pairs. The spectral features of free ctDNA and PE−ctDNA complex are shown in Figure 9A. The peak at 1717 cm^{-1} is attributed to the guanine (G) in plane-stretching vibrations. The 1667 cm^{-1} peak corresponds to thymine (T) stretching. The vibrational bands at 1610 and 1490 cm^{-1} are assigned to adenine (A) and cytosine (C) nitrogenous bases, respectively. Bands at 1222 and 1088 cm^{-1} denote phosphate asymmetric and symmetric vibrations, respectively.[45,46]

It was observed that at low PE concentration (r = 1/200), the guanine peak at 1717 cm^{-1} shifted downward to 1710 cm^{-1}, and the cytosine peak at 1490 cm^{-1} shifted upward to 1492 cm^{-1}, indicating PE started to react with the G−C base pairs of ctDNA. Shifts for phosphate asymmetric stretching from 1222 to 1220 cm^{-1} and symmetric stretching from 1088 to 1086 cm^{-1} suggest that there were some weak external interactions of PE with the phosphate backbone upon its interaction with the ctDNA double helix.[47] The major intensity increases (Figure 9B) were attributed to a partial helix destabilization induced by the PE−ctDNA interaction.[48]

As PE concentration increased (r = 1/100), the main thymine vibration at 1667 cm^{-1} of free ctDNA shifted toward a higher frequency at 1669 cm^{-1}, which proved PE could slightly interact with thymine O-2.[49] Besides, the further shift in position and decrease in intensity of base vibration of cytosine demonstrated the existence of interaction between the planar aromatic rings of PE and heterocyclic base pairs of ctDNA.[49] At high PE concentration (r = 1/50, 1/25), observed changes for the guanine band from 1710 to 1709 cm^{-1}, the adenine band from 1610 to 1612 cm^{-1}, and the cytosine band from 1493 to 1495 cm^{-1} could be related to PE interacting with G−C and

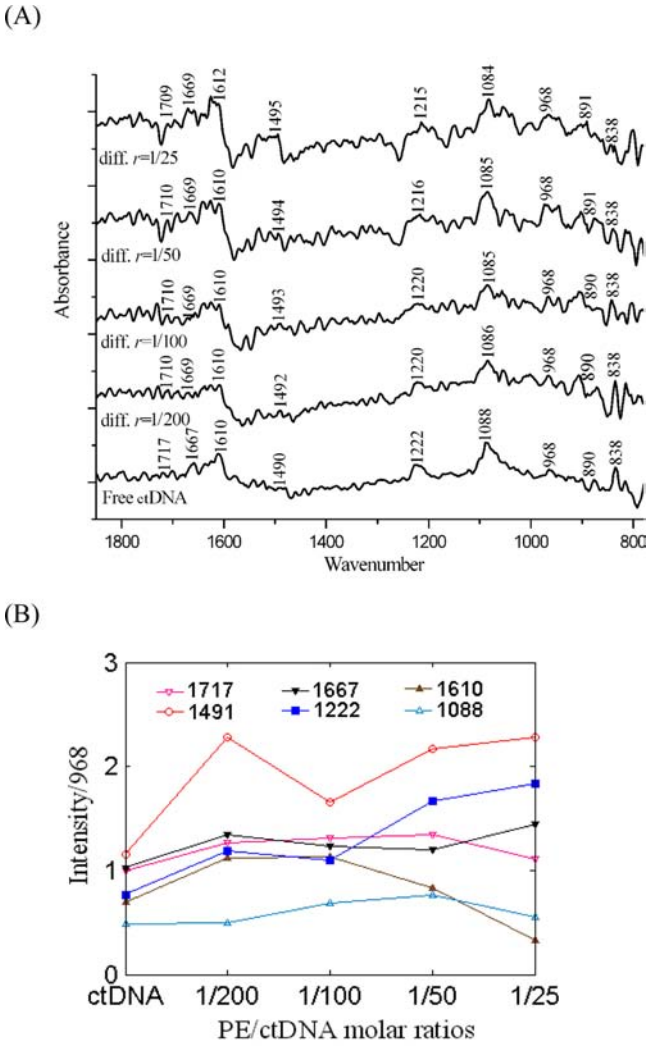

Figure 9. (A) FT−IR spectra and difference spectra [(ctDNA + PE) − PE solution] in the region of 1800−800 cm^{-1} for free ctDNA and PE−ctDNA complex in an aqueous solution. (B) Intensity ratio variations of several ctDNA in-plane vibrations as a function of different PE/ctDNA molar ratios.

A−T base pairs. Considering changes in position and intensity of ctDNA vibration bands, the G−C base pairs were more prone to perturbation and interacted with PE aromatic ring, which was able to offer steric advantages for the molecular interaction.[47] In addition, the phosphate asymmetric stretching and symmetric stretching shifted to lower frequency accompanied by intensity changes. According to the analysis of CD spectra, the interaction led to alteration of the conformation of normal DNA to a more highly wound form of B-DNA. The conformation transformation caused differences in the state of phosphate group, which induced the changes mentioned above. The consistency of B-DNA marker peaks at 838 and 890−891 cm^{-1} was perfectly corresponded to preservation of B-conformation.

Molecular Modeling Studies. Molecular docking can provide some insight into the interactions of macromolecules with ligands and preferred binding mode with the help of a variety of docking programs. To determine the preferred binding sites on DNA, PE was docked to the DNA, and the results are presented in Figure 10. Through the docking method, 100 multimember conformational clusters correspond-

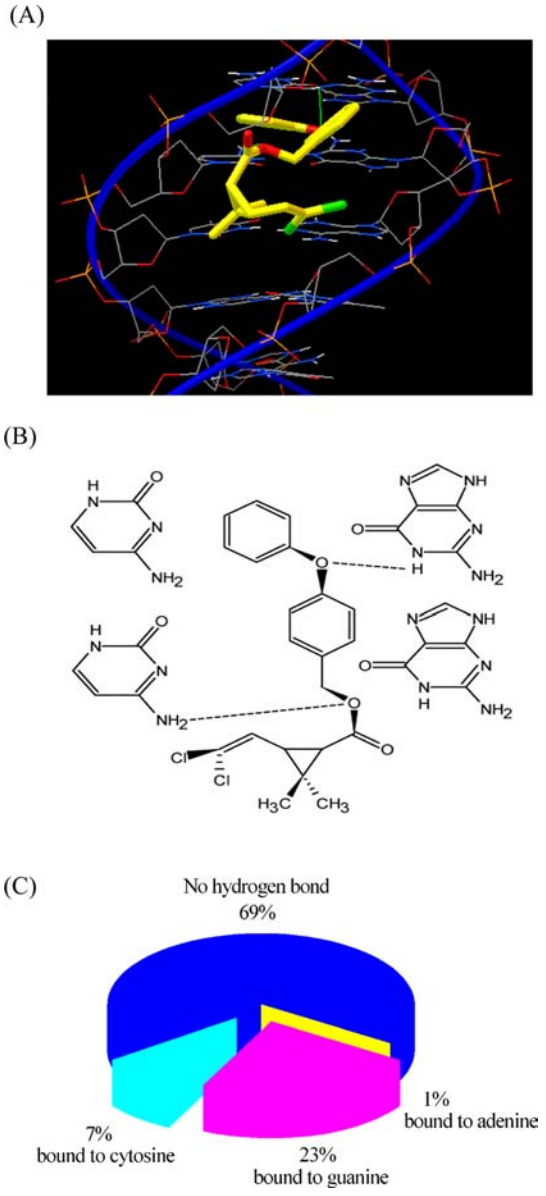

Figure 10. (A) Docking pose of the energy-minimized structure of PE−ctDNA complex. (B) Hydrogen bonds (dashed line) between PE and base pairs. (C) Proportional distribution of hydrogen bond formed between PE and different bases.

ing to the lowest free energy of binding were obtained after performing, and the optimal geometry of the complex was selected to discuss.

As shown in Figure 10A, the A ring of PE was capable of inserting into the intermediate space of the two base pairs in a parallel configuration, while the B ring of PE was ready to obliquely intercalate into the space of two base pairs. Moreover, two hydrogen bonds formed between G−C base pairs (Figure 10A, green line). Figure 10B clearly showed that the oxygen atom O-20 of the PE molecule could form a hydrogen bond with the hydrogen atom associated with N-1 of guanine (DG16 of A-chain) and oxygen atom O-12 of PE built a hydrogen bond with H-41 attached to N-4 of cytosine (DC8 of B-chain). Among the 100 conformational clusters, in 69% of the geometries PE did not form any hydrogen bond with the DNA, while 23% can form a hydrogen bond with guanine and 7% with cytosine (Figure 10C). However, only the remaining 1% geometry showed PE built a hydrogen bond with adenine. This docking result explained well that PE was prone to bind to G−C base pairs of ctDNA, which verified the conclusion of FT−IR analysis.

In conclusion, UV−vis absorption, fluorescence, CD, and FT−IR spectroscopy, coupled with viscosity experiments, were applied to investigate the binding between permethrin (PE) and ctDNA with the aid of the chemometrics method, MCR−ALS. The results suggested that the most probable mechanism of ctDNA interaction with PE was intercalation, and PE most likely bound to G−C base pairs of the DNA which was corroborated by the docking studies. This binding induced a more highly wound form of B-conformation of DNA. The application of the MCR−ALS for the resolution of the expanded UV−vis and fluorescence spectroscopic data matrix produced the estimates of the pure spectra for PE and ctDNA, which were in good accordance with the measured responses. And importantly, the spectrum of the interaction product, PE−ctDNA, was extracted. The concentration profiles for the three reaction components (PE, ctDNA, and PE−ctDNA complex) were also simultaneously obtained. The results showed significant potential for investigating the mechanism of the interaction of target DNA with small compounds at the molecular level.

AUTHOR INFORMATION

Corresponding Author

*Tel.: +8679188305234. Fax: +8679188304347. E-mail address: gwzhang@ncu.edu.cn.

Notes

The authors declare no competing financial interest.

ACKNOWLEDGMENTS

This study was supported financially by The National Natural Science Foundation of China (Nos. 21167013 and 31060210), the Supported Program of Science and Technology of Jiangxi Province (2009BNA09000 and 20112BBF60010), the Natural Science Foundation of Jiangxi Province (20114BAB204019), and the Open Project Program and Objective-Oriented Project of State Key Laboratory of Food Science and Technology of Nanchang University (SKLF-KF-201203 and SKLF-MB-201002).

REFERENCES

(1) Chen, Q. Y.; Li, D. H.; Zhao, Y.; Yang, H. H.; Zhu, Q. Z.; Xu, J. G. Interaction of a novel red-region fluorescenct probe, Nile Blue, with DNA and its application to nucleic acids assay. *Analyst* **1999**, *124*, 901−906.

(2) Sahoo, B. K.; Ghosh, K. S.; Bera, R.; Dasgupta, S. Studies on the interation of diacetylcurumin with calf thymus DNA. *Chem. Phys.* **2008**, *35*, 1−3.

(3) Sun, Y. T.; Bi, S. Y.; Song, D. Q.; Qiao, C. Y.; Mu, D.; Zhang, H. Q. Study on the interaction mechanism between DNA and the main active components in Scutellaria baicalensis Georgi. *Sens. Actuators, B* **2008**, *129*, 799−810.

(4) Zhang, Y.; Wang, X. M.; Ding, L. S. Interaction between tryptophan−vanillin Schiff base and herring sperm DNA. *J. Serb. Chem. Soc.* **2010**, *75*, 1191−1201.

(5) Long, Y. T. Identification of bio-macromolecular (DNA and protein) adducts by mass spectrometry. *Chin. J. Environ. Sci.* **1995**, *16*, 79−82.

(6) Punareewattana, K.; Smith, B. J.; Blaylock, B. L.; Longstreth, J.; Snodgrass, H. L. Topical permethrin exposure inhibits antibody

production and macrophage function in C57Bl/6N mice. *Food Chem. Toxicol.* **2001**, *39*, 133−139.
(7) Shah, P. V.; Monroe, R. J.; Guthrie, F. E. Comparative rates of dermal penetration of insecticides in mice. *Toxicol. Appl. Pharmacol.* **1981**, *59*, 414−423.
(8) Sidon, E. W.; Moody, R. P.; Franklin, C. A. Percutaneous absorption of cis- and trans-permethrin in rhesus monkeys and rats: Anatomic site and interspecies variation. *J. Toxicol. Environ. Health* **1988**, *23*, 207−216.
(9) Taplin, D.; Terro Lynn Meinking, B. A.; Joaquin, A.; Chen, M. D.; Regulo Sanchez, M. D. Comparison of crotamiton 10% cream (Eurax) and permethrin 5% cream (Elimite) for the treatment of scabies in children. *Pediatric Dermatol.* **1990**, *7*, 67−73.
(10) Institóris, L.; Ųndeger, Ų.; Siroki, O.; Nehéz, M.; Dési, I. Comparison of detection sensitivity of immuni- and genotoxicological effects of subacute cypermethrin and permethrin exposure in rats. *Toxicology* **1999**, *137*, 47−55.
(11) Zhang, G. W.; Fu, P.; Wang, L.; Hu, M. M. Molecular spectroscopic studies of farrerol interaction with calf thymus DNA. *J. Agric. Food Chem.* **2011**, *59*, 8944−8952.
(12) Charak, S.; Jangir, D. K.; Tyagi, G.; Mehrotra, R. Interaction studies of Epirubicin with DNA using spectroscopic techniques. *J. Mol. Struct.* **2011**, *1000*, 1−3.
(13) Ni, Y. N.; Wei, M.; Kokot, S. Electrochemical and spectroscopic study on the interaction between isoprenaline and DNA using multivatiate curve resolution−alternating least squares. *Int. J. Biol. Chem.* **2011**, *49*, 622−628.
(14) Ni, Y. N.; Wang, Y. X.; Kokot, S. Study of the interaction between 10-hydrixycamptothecine and DNA with the use of ethidium bromide dye as a fluorescence probe. *Sens. Actuators, B* **2011**, *156*, 290−297.
(15) Kanakis, C. D.; Nafisi, Sh.; Rajabi, M.; Shadaloi, A.; Tarantilis, P. A.; Polissiou, M. G.; Bariyanga, J.; Tajmir-Riahi, H. A. Structural analysis of DNA and RNA interactions with antioxidant flavonoids. *Spectroscopy* **2009**, *23*, 29−43.
(16) Shahabadi, N.; Fatahi, A. Multispectrocopic DNA-binding studies of a tris-chelate nickel(II) complex containing 4,7-diphenyl 1,10-phenanthroline ligands. *J. Mol. Struct.* **2010**, *970*, 90−95.
(17) Zhao, N.; Wang, X. M.; Pan, H. Z.; Hu, Y. M.; Ding, L. S. Spectroscopic studies on the interaction between tryptophan−erbium(III) complex and herring sperm DNA. *Spectrochim. Acta, Part A* **2010**, *75*, 1435−1442.
(18) Charak, S.; Shandilya, M.; Tyagi, G. J.; Mehrotra, R. Spectroscopic and molecular docking studies on chlorambucil interaction with DNA. *Int. J. Biol. Macromol.* **2012**, *51*, 406−411.
(19) Berman, H. M.; Westbrook, J.; Feng, Z. K.; Gilliland, G.; Bhat, T. N.; Weissig, H.; Shindyalov, L. N.; Bournel, P. E. The Protein Data Bank. *Nucleic Acids Res.* **2000**, *28*, 235−242.
(20) Sun, Y. J.; Ji, F. Y.; Liu, R. T.; Lin, J.; Xu, Q. F.; Gao, C. Z. Interaction mechanism of 2-aminobenzothiazole with herring sperm DNA. *J. Lumin.* **2012**, *132*, 507−512.
(21) Ricci, C. G.; Netz, P. A. Docking studies on DNA−ligand interactions: Building and application of a protocol to identify the binding mode. *J. Chem. Inf. Model* **2009**, *49*, 1925−1935.
(22) Tauler, R.; Lzquier-Ridorsa, A.; Casassas, E. Simultaneous analysis of several spectroscopic titrations with self-modelling curve resolution. *Chemom. Intell. Lab. Syst.* **1993**, *18*, 293−300.
(23) Tauler, R. Multivariate curve resolution applied to second order data. *Chemom. Intell. Lab. Syst.* **1995**, *30*, 133−146.
(24) Golub, G. H.; Loan, C. F. V. *Matrix Computations*; John Hopkins Press Ltd: London, U.K., 1989.
(25) Maeder, M. Evolving factor analysis for the resolution of overlapping chromatographic peaks. *Anal. Chem.* **1987**, *59*, 527−530.
(26) Gampp, H.; Maeder, M.; Meyer, C. J.; Zuberbühler, A. D. Calculation of equilibrium constants from multiwavelength spectroscopic data−IV: Model-free least-squares refinement by use of evolving factor analysis. *Talanta* **1986**, *33*, 943−951.
(27) Windig, W.; Guilment, J. Interactive self-modeling mixture analysis. *Anal. Chem.* **1991**, *63*, 1425−1432.
(28) Zhang, Q. L.; Ni, Y. N.; Kokot, S. Molecular spectroscopic studies on the interaction between Ractopamine and bovine serum albumin. *J. Pharm. Biomed. Anal.* **2010**, *52*, 280−288.
(29) Wang, F.; Huang, W.; Su, L.; Dong, Z. J.; Zhang, S. Spectrofluorimetric study of the binding of codeine to nucleic acids. *J. Mol. Struct.* **2009**, *927*, 1−6.
(30) Zhong X. Z. *Chemometrics-spectrum method study interaction mechanism of small drug molecules with DNA*. Dissertation, Nanchang University, Nanchang, 2007.
(31) Chen, Z. G.; Zhang, G. M.; Chen, X.; Gao, W. H. A resonance light-scattering off−on system for studies of the selective interaction between adriamycin and DNA. *Anal. Bioanal.Chem.* **2012**, *402*, 2163−2171.
(32) Štefanišinová, M.; Tomečková, V.; Kožurková, M.; Ostró, A.; Mareková, M. Study of DNA interactions with cyclic chalcone derivatives by spectroscopic techniques. *Spectrochim. Acta, Part A* **2011**, *81*, 666−671.
(33) Shahabadi, N.; Maghsudi, M.; Kiani, Z.; Pourfoulad, M. Multispectroscopic studies on the interaction of 2-tert-butylhydroquinone (TBHQ), a food additive, with bovine serum albumin. *Food Chem.* **2011**, *124*, 1063−1068.
(34) Lakowicz, J. R. *Principles of Fluorescence Spectroscopy*, 3rd ed; Springer Publications: New York, 1990.
(35) Yang, M. M.; Xiao, Q.; Xi, X. L. Study of the interaction of cephalosporin class medicine with albumin by fluorescence enhancement and fluorescence quenching theories. *Chin. J. Chem.* **2006**, *24*, 642−648.
(36) Ross, P. D.; Subramanian, S. Thermodynamics of protein association reactions: Forces contributing to stability. *Biochemistry* **1981**, *20*, 3096−3102.
(37) Kashanian, S.; Dolatabadi, J. E. N. In vitro studies on calf thymus DNA interaction and 2-tert-butyl-4-methylphenol food additive. *Eur. Food Res. Technol.* **2010**, *230*, 821−825.
(38) Akbay, N.; Seferoğlu, Z.; Gők, E. Fluorescence interaction and determination of calf thymus DNA with two ethidium derivatives. *J. Fluoresc.* **2009**, *19*, 1045−1051.
(39) Devi, V. Ch.; Singh, N. R. Absorption spectroscopic probe to investigated the interaction between Nd(III) and calf-thymus DNA. *Spectrochim. Acta, Part A* **2011**, *78*, 1180−1186.
(40) Shahabadi, N.; Maghsudi, M.; Mahdavi, M.; Pourfoulad, M. Interaction of calf thymus DNA with the antiviral drug lamivudine. *DNA Cell. Biol.* **2011**, *31*, 122−127.
(41) Ma, Y. D.; Zhang, G. W.; Pan, J. H. Spectroscopic studies of DNA interactions with food colorant indigo carmine with the use of ethidium bromide as a fluorescence probe. *J. Agric. Food. Chem.* **2012**, *60*, 10867−10875.
(42) Wang, J.; Yang, Z. Y.; Yi, X. Y.; Wang, B. D. DNA-binding properties studies and spectra of a novel fluorescent Zn(II) complex with a new chromone derivative. *J. Photochem. Photobiol., A* **2009**, *201*, 2−3.
(43) Snelders, D. J. M.; Casini, A.; Edafe, F.; Koten, G. V.; Gebbink, R. J. M. K.; Dyson, P. J. Ruthenium(II) arene complexes with oliglcationic triarylphosphine ligands: Synthesis, DNA interaction and in vitro properties. *J. Organomet. Chem.* **2011**, *696*, 1108−1116.
(44) Chen, H. M.; Parkinson, J. A.; Parsons, S.; Coxall, R. A.; Gould, R. O.; Sadler, P. J. Organometallic ruthenium(II) diamine anticancer complexes: Arene-nucleobase stacking and stereospecific hydrogen bonding in guanine adducts. *J. Am. Chem. Soc.* **2002**, *124*, 3064−3082.
(45) Nafisi, S.; Saboury, A. A.; Keramat, N.; Neault, J. F.; Tajmir-Riahi, H. A. Stability and structural features of DNA intercalation with ethidium bromide, acridine orange, and methylene blue. *J. Mol. Struct.* **2007**, *827*, 35−43.
(46) Jangir, D. K.; Charak, S.; Mehrotra, R.; Kundu, S. FTIR and circular dichroism spectroscopic study of interaction of 5-flurouracil with DNA. *J. Photochem. Photobiol., B* **2011**, *105*, 143−148.
(47) Saito, S. T.; Silva, G.; Pungartrik, C.; Brendel, M. Study of DNA−emodin interaction by FTIR and UV−vis spectroscopy. *J. Photochem. Photobiol., B* **2012**, *111*, 59−63.

(48) Nafisi, S.; Manouchehri, F.; Tajmir-Riahi, H. A.; Varacipour, M. Structural features of DNA interaction with caffeine and theophylline. *J. Mol. Struct.* **2008**, *875*, 1−3.
(49) Tyagi, G.; Charak, S.; Mehrotra, R. Binding of an indole alkaloid, vinblastine to double stranded DNA: A spectroscopic insight into nature and strength of interaction. *J. Photochem. Photobiol., B* **2012**, *108*, 48−52.